Microstructural aspects of the transition between two regimes in orthogonal cutting of AISI 1045 steel

Bentejui Medina-Clavijo[a, b]

Mikel Saez-de-Buruaga[a]

Christian Motz[d]

Daniel Soler[a]

Andrey Chuvilin[b, c, *]

a.chuvilin@nanogune.eu

Pedro J. Arrazola[a]

[a]Faculty of Engineering, Mondragon Unibertsitatea, 20500 Arrasate, Spain

[b]Electron-Microscopy Laboratory, CIC nanoGUNE Consolider, 20018 Donostia, Spain

[c]Ikerbasque, Basque Foundation for Science, 48013 Bilbao, Spain

[d]Department of Material Science and Methods (MWW), Saarland University, Saarbrücken D-66041, Germany

*Corresponding author at: CIC NanoGUNE Consolider, Tolosa Hiribidea 76, E-20018 Donostia - San Sebastian, Spain.

Abstract

In depth understanding of tool-chip friction behavior is a significant aspect for tool wear performance in steels. In the present work attention has been paid to the strain mode of the chip section in contact with the rake surface of the tool, and its influence on the mechanics of material removal. There is a multitude of evidence for the existence of qualitatively different cutting regimes in orthogonal machining of annealed AISI-1045 steel with uncoated P15 carbide cutting tools in dry conditions at cutting speeds between 5 and 200 m/min. The evaluation of chip morphology and microstructure, and cutting and feed forces, revealed an abrupt step-like transition at a cutting speed in the range of 50–60 m/min, which was attributed to the transition from built-up edge (BUE) mode developed at low cutting speed, to the mode at which the chip slides directly over the tool surface. These qualitatively distinct mechanisms of tool-chip interaction are determined by two different microstructural effects: work hardening by severe plastic deformation and microstructural softening by dynamic recrystallization (DRX). It is argued that the onset of DRX is the reason for further instability of BUE and thus is the main cause of change of the cutting regime.

Keywords: Machining; Cutting; Microstructure; Dynamic recrystallization; Built-up edge; AISI 1045

1 Introduction

Understanding the phenomena occurring in the tool-chip contact area is a key for improving the machining process. Tool wear, and subsequently tool life, are notoriously affected by the thermomechanical loads occurring in this zone. However, direct experimental assessment of the conditions in the tool-chip contact area during machining presents two major challenges: (i) the small dimensions where the phenomena are occurring and (ii) the extreme values of strain, strain-rate, temperature, pressure and stress reached. Although recently Arrazola et al. (2015) and Lee et al. (2006) have provided new insights for experimental assessment of values for temperature and strain respectively, there is still a shortage of quantitative experimental data available for the other parameters. Variables like pressure or stress are inaccessible by the existing experimental measurement techniques. This fact hampers an in-depth analysis of what happens directly at the tool-chip contact area. There has been a substantial effort devoted to studies aiming to understand tool-chip processes. Jaspers and Dautzenberg (2002) described non-linear friction effects that are dependent on cutting speed, which have been studied by Seker et al. (2004) by varying the feed rate. Ben Abdelali et al. (2012) pointed out the existence of tribological regimes when studying the contact between tool and workpiece material. Moreover, Rech et al. (2013) identified different regimes in the case of AISI 1045, AISI 4142, AISI 304 L steels, leading to different scenarios in the chip-tool interaction, potentially leading to either discontinuous chip formation and a rough workpiece finish at low cutting speeds, or to a continuous chip and smooth finishing at high speeds. Besides giving a clear link between input and output parameters of the processes, classical

macroscopic characterization techniques were not able to disclose the microscopic mechanisms for the observed phenomena, and thus to gain a fundamental understanding of the processes underlying complex manufacturing processes.

To face the above challenges, an in-depth study of the chip microstructure, as it was shown by Courbon et al.(2013), could be a solution. Though the chip is considered to be waste in the machining process, it stores the distinct signatures of the conditions that were present at the moment of cutting, especially in the secondary shear zone (SSZ), which has been in the direct contact to the tool.

Several authors have assessed the structure of SSZ of the chips at the microscopic scale after machining steels. It was shown that the crystal structure in the SSZ of the chip in the proximity of the rake surface presents a particular grain shape and distribution. Wallbank (1979) found that at low cutting speed the material is refined, laminated and hardened, leading to depositions at the tool edge, the so called “built-up edge” (BUE) phenomenon. In contrast, at higher speed (starting from 50- to 60 m/min) these depositions disappear and the chip slides directly against the tool. Courbon et al. (2013) pointed out that in that case the grains of SSZ are refined to about 200 nm and tend to equiaxity in the proximity of the tool, in contrast to the rest of the chip. Griffiths (1987) reported about white layers in this part of the chip, since it appears as a bright band near the chip surface in optical images. Pu et al. (2015) proposed that the appearance of equiaxial grains in SSZ may be due to recrystallization or phase transition, and this recrystallization in turn was utilized to explain softening effects appearing in the material during high speed machining. Jaspers and Dautzenberg (2002) pointed out that these phenomena depend on the cutting speed and take place only in certain chip locations. The main challenge in characterization of the structure of material in SSZ is the size of the grains often going below 100 nm. This makes high resolution techniques like electron microscopy the only option for addressing this challenge. Due to complexity and limited availability of such methods for the metalworking community, structural and mechanical characterization works have been separated and thus an important link between the structure, material properties and machining conditions has not yet been clearly established.

In this work a composite study is presented, which includes characterization of the evolution of microstructure in the SSZ with the cutting speed and its correlation with parameters of the cutting process such as chip morphology, cutting and feed forces, chip/tool temperature and tool-chip contact length. In agreement with previous works an abrupt transition of the tool-tip interaction regime at ~50 m/min cutting speed is observed and correlated to the microstructure evolution; the microscopic nature of above transition is discussed.

2 Experimental procedure

2.1 Machining

Bars of AISI 1045 annealed steel with 58 mm diameter were employed in this study. The material had a hardness of 300HB, a mean grain size of 7-9 μm, and microstructure of 75% perlite and 25% ferrite.

Orthogonal cutting tests were performed in a vertical milling machine using tubular samples that were 65 mm long, 58 mm in outer diameter, and 2 mm in thickness with a 15 mm long solid base for clamping (see Fig. 1 for schematics of the set up). Tests were carried out in dry conditions with uncoated P15 grade carbide cutting tools, reference WIDIA TPUN 160308 TTM (rake angle = 6 degrees and cutting edge radius = 40 μm). The feed rate was kept constant to 0.2 mm/rev, while the cutting speed was varied: 5, 10, 25, 50, 75, 100 and 200 m/min. Three trials of every experiment were carried out in order to determine repeatability. A fresh cutting edge was used for each test to prevent wear effects. For every cutting experiment feed and cutting force, tool tip temperature, chip morphology and thickness, chip microstructure and tool-chip contact length were monitored. A Kistler 9121 dynamometer was used to measure the cutting and feed forces at a sampling rate of 5000 Hz and a 300 Hz cut-off filter. The tool and tool holder were mounted on the dynamometer. The dynamometer was fixed to the table of the machine as well as the infrared camera (upper sketch). In the same way as Armendia et al. (2010), the workpiece was clamped to the machine spindle, which provided the rotational movement and vertical feed. While the tool remained fixed, the workpiece turned to generate the chip perpendicularly to the camera (bottom sketch).

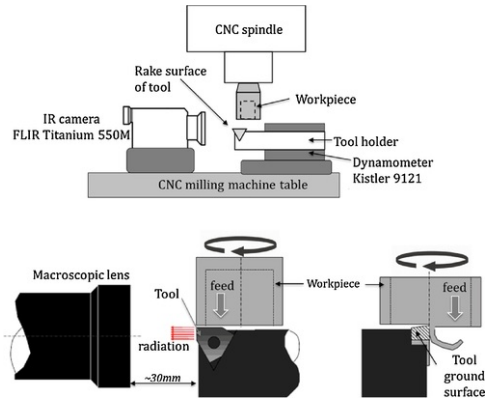

Fig. 1 Experimental set-up for orthogonal cutting tests.

alt-text: Fig. 1

The temperature was measured by a FLIR Titanium 550 M infrared camera mounted to the machine table. The camera was equipped with a macroscopic lens giving a spatial resolution of 1 pixel = 10 µm. A narrow-band filter in the IR spectral range of 3.97–4.01 µm was applied. In order to have sufficient data to evaluate the temperature evolution over time, it is necessary to have a high acquisition frame rate (*fr*). However, a high *fr* implies reducing the camera resolution and therefore the field of vision. In the present study the frame rate was *fr* = 1000 Hz which allowed thermographies of 160 × 128 pixels to be recorded.

To prevent a nonlinear detector response, the integration time was selected depending on radiation values as 60, 100, 200, 300 and 150 µs (without filter for a v_c = 5 m/s). The cutting time for each test was 5 s, which was long enough to ensure a temperature steady state condition and short enough to prevent oxidation on the tool insert. In order to relate the camera recorded data with the real temperature the calibration method proposed by Soler et al. (2018) was followed. The tool temperature was measured on the tool ground face (see Fig. 2a). In order to estimate the temperatures on the mid-plane of the rake face (see Fig. 2b) two approximations were applied. First, based on the experimental procedure developed by Soler et al. (2015), the temperature from the tool side was interpolated to the contact initiation section. As a result, the effect of the overhang distance (d on Fig. 2b) was corrected from d = 0.3 mm to d = 0 mm. Secondly, based on the analysis carried out by Arrazola et al. (2015), the previously corrected temperature was multiplied by a ratio to take into account the increase in the tool temperature from the contact initiation section to the middle section due to the friction effects. From the results obtained by Arrazola et al. 2015 it was determined that there was a temperature increase from the contact initiation section to the mid-plane of the rake face of 10% for a cutting speed of 75 m/min and an increase of 25% for 250 m/min in the case of an AISI-4140 steel. According to those published results, previously corrected experimental temperatures were increased by 10~~-25% depending on the cutting condition.The chip thickness was measured from low magnification SEM images of polished chip cross-sections. Tool-chip contact length was measured from the contact marks on the tool, see the information in the appendix for details.The measurement uncertainties were ± 10 N in forces, ±~~ -25% depending on the cutting condition.

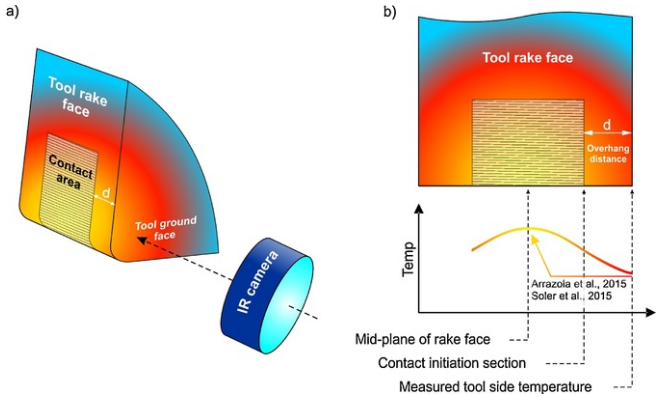

Fig. 2 a) Schematic view of tool and camera for infrared photography of tool side face. b) Temperature correction from tool side to the mid plane of the rake face.

alt-text: Fig. 2

The chip thickness was measured from low magnification SEM images of polished chip cross-sections. Tool-chip contact length was measured from the contact marks on the tool, see the information in the appendix for details.

The measurement uncertainties were ±10 N in forces, ±100 °C in tool temperature, ~~± 0.02 mm in chip thickness and ±~~ ±0.02 mm in chip thickness and ±0.2 mm in tool contact length.

2.2 Modeling

A model set-up in Abaqus/Explicit™ (v6.14) described by Arrazola et al. (2007) was employed to obtain quantitative information of cutting and feed forces, temperatures and plastic strain. Coupled mechanical and thermal analysis was done using the Arbitrary Lagrangian Eulerian (ALE) formulation.

Material behavior was determined by a Johnson-Cook flow stress model. The parameters of the constitutive model were characterized with experimental dynamic compression tests, as described in previous work of Saez-de-Buruaga et al. (2017).

The Coulomb friction law governs mechanical aspects at the tool-chip interface contact in sliding regime. The friction was identified as being dependent on the sliding velocity between tool and workpiece based on the work of Ben Abdelali et al. (2012) and Rech et al. (2013). The values of friction were set in between $\mu = 0.8$–0.55 for sliding velocities in the range of 10–300 m/min. Heat transfer was allowed at the tool chip contact area and at the backside of the tool. Following the method proposed by Saez-de-Buruaga et al. (2017), workpiece material and tool thermal properties were characterized as functions of temperature. Fig. 3 illustrates the steady state temperature distribution in the chip, based on the conditions detailed above for the case of cutting at 75 m/min. Note the particularly refined mesh applied in the tool edge contact in order to counteract the large gradients of the variables analyzed in this area.

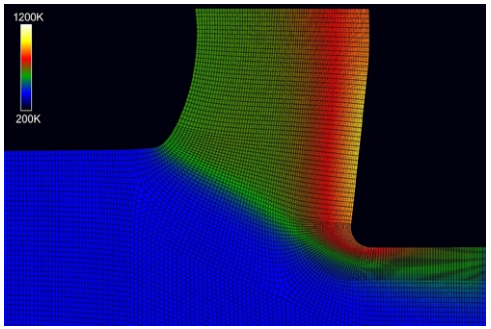

Fig. 3 Temperature distribution obtained in FEM for Steel 1045 when machining at 75 m/min.

alt-text: Fig. 3

In order to reduce the computational time, the mass scaling option was used, which basically increases material density in a controlled manner to increase a stable-time increment. A numerical comparison carried out to verify differences when using this option showed differences lower than 1% in the most relevant variables like temperature, cutting forces or Von Mises stresses. The option “variable mass scaling” proposed in Abaqus/Explicit™ (v6.14) was set up so as the lower time increment attained the value of 10^{-9} s. This option allowed reducing computational time by more than 10 times as it was shown by Arrazola et al. (2007).

Entry parameters for material, contact and cutting process are shown in Table A2 of the appendix.

2.3 Sample preparation and microscopy

A sample of workpiece material was diced by diamond saw and the surface was polished with diamond lapping films and an aluminum oxide suspension. A final chemical-mechanical polishing was made using a silica polishing suspension (Struers OPS nondry). In order to prepare the chip cross sections, chips were embedded in conductive silver epoxy (Chemtronics CW2400). This reduces drift and sample charging in the electron microscope as compared to a standard epoxy. Then the embedded chips were polished using the same procedure as for the workpiece material.

Chip surfaces that had been in contact with the tool were optically examined with a Leica DM4000 M microscope. The microstructure of the workpiece and chip was studied by scanning electron microscopy (SEM) and focused ion beam (FIB) techniques using a DualBeam SEM/FIB instrument (Helios 600 NanoLab, FEI Co.). SEM was used to reveal the major morphological features of the samples like the shape of the interface surfaces and cracks. The crystallinity of the samples, i.e. the size and the shape of crystallites, was studied as by Canovic et al. (2008) by exploiting FIB imaging utilizing channeling contrast. It was found that the ion beam produces substantially higher channeling contrast than the electron beam, yet preserving sufficient resolution at low beam currents (1.5–~~40~~ 40 pA). 5 kV acceleration voltage for electron beam and 30 kV for the ion beam were used.

The electron backscatter diffraction (EBSD) technique was used to build maps of the crystallographic orientation, texture and kernel average misorientation. For this analysis a ZEISS Sigma SEM equipped with a NordlysNano EBSD camera from Oxford Instruments was used. Scanning was performed at 20 kV acceleration voltage and a step size of 50 nm. Subsequent data analysis was made by OIM analysis software.

3 Results

This work presents a multi-approach study. On the one hand, the material was observed before and after machining by optical and electron microscopy. On the other hand, multiple characteristics and parameters were measured during machining experiments: feed force (F_f), cutting force (F_c) and chip thickness (t). Fig. 4 gives a schematic of the parameters being monitored and their relation to the particular parts of experimental setup.

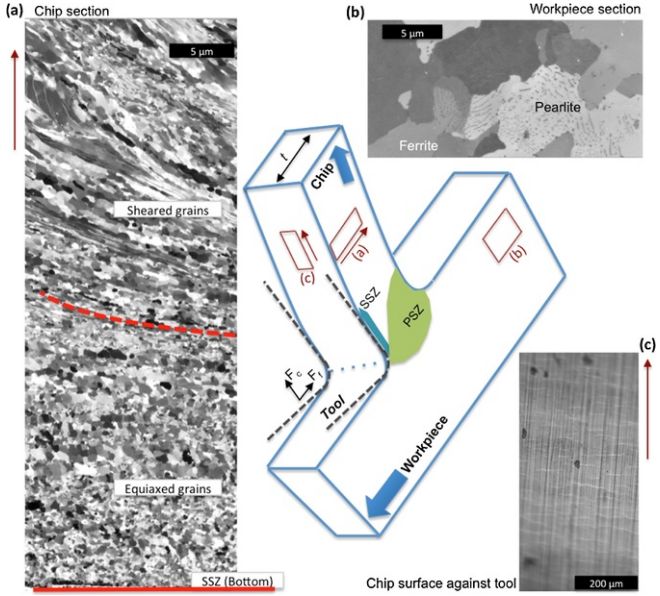

Fig. 4 In the middle is a sketch of different areas and parameters of the chip under study. (a) Ion image of the chip cross-section when machining at 100 m/min. Red dashed line is an estimation of PSZ - SSZ boundary. (b) Ion image of the workpiece section. (c) Optical image of the chip surface sliding against tool when machining at 100 m/min (For interpretation of the references to colour in this figure legend, the reader is referred to the web version of this article).

alt-text: Fig. 4

The analysis of the chip (Fig. 4a) was made by FIB imaging. The same technique was used to study the workpiece microstructure (Fig. 4b). Chip rake surface morphology was observed by optical microscopy (Fig. 4c).

The typical FIB image of the microstructure of a workpiece sample before machining is depicted in Fig. 4b. Pearlite colonies cover 75 % of the sample area. Most of the colonies are constituted of lamellar pearlite. However, around 25 % of pearlite develops some degradation, i.e. lamellar discontinuity and fragmentation.

Fig. 4a shows an overview FIB image of the cross-section of a chip machined at 100 m/min. The surface that has been in contact with the tool is at the bottom of the image. A characteristic feature of the structure is pronounced shape anisotropy, with the long axis of the crystals changing direction from the shear angle of the PSZ to angles almost parallel to the surface in the proximity of SSZ. The other peculiar structural feature is the existence of the so called “white layer” (the name coming from optical images of cross-sections) – the area at the tool-chip contact surface where, as reported by Courbon et al. (2013), crystallites are very small and do not show pronounced shape anisotropy. Hereafter, this area will studied, as it is particularly this, which reflects specific thermomechanical conditions of the cutting process at the very proximity of the tool. Fig. 4c gives an example of an optical image of the chip surface at the rake side of the chip produced at 100 m/min cutting speed.

3.1 Microscopy

Fig. 5 summarizes morphological and structural features of the chips obtained at different cutting velocities. The left column depicts optical images of the bottom chip surface that has been in contact with the rake surface (corresponding to position of Fig. 4c). There are two different morphologies present: at 50 m/min and above the chips are smooth and are not fragmented; however, at cutting speeds of 25 m/min and below the chip surface develops

cracks perpendicular to the direction of the chip movement. In the middle column optical images of the cross-sections reveal a typical lamellar structure characteristic for the PSZ. The lamellae direction is changing from parallel to the surface at the tool-chip interface to its bulk value, which is specific for every cutting speed.

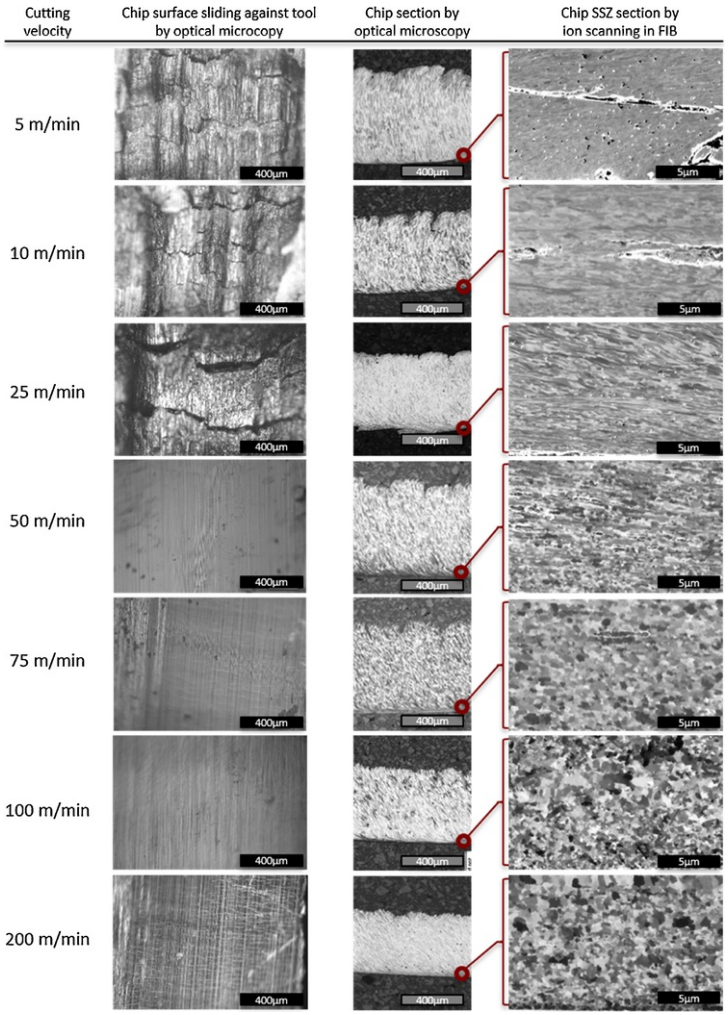

Fig. 5 Chips made by cutting with a feed of 0.2 mm and cutting speeds from 5 to 200 m/min. Left column - images of the chip surface sliding against the tool (location of Fig. 4c). Middle column – optical images of the complete chip cross-section. Right column - FIB images of the SSZ area (the bottom corresponds to the chip rake surface) (location of this area is indicated on Fig. 4a).

alt-text: Fig. 5

The right column of Fig. 5 depicts FIB images of the chip cross-section of the area in the proximity of the rake surface, which reveal the grain distribution down to sub-100 ~~nanometer~~ nm size in the SSZ at the tool-chip interface (corresponding to the position of Fig. 4a). For chips cut at 25 m/min and below the grains in this region develop a lamellae type structure with a strong shape anisotropy. In the vicinity of the tool-chip interface the lamellae are almost parallel to the surface. Furthermore, in chips machined at low speed the features directly related to BUEs can be observed. Fig. 6 shows a complete BUE, which was detached from the tool tip and was trapped inside the chip when machining at 5 m/min. The image reveals a severely deformed microstructure in the BUE and in the vicinity of the tool. It is notable that the lamellae structure is significantly finer inside the BUE than in the rest of the chip. Similar signatures of BUE were present also at 10 and 25 m/min cutting speeds. In addition, Fig. 6 demonstrates a change in the cutting geometry, as in the presence of BUE the chip slides against a nose with an angle of 20 degrees instead of

the rake angle of the tool of 6 degrees.

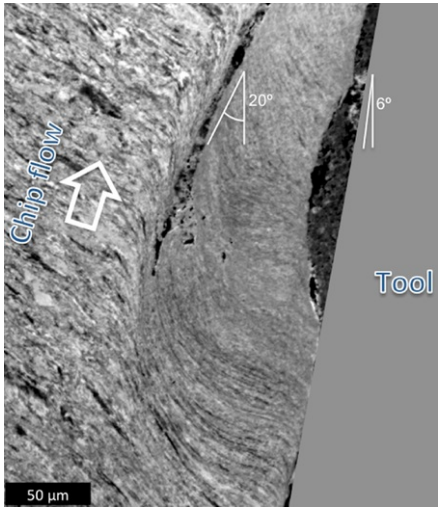

Fig. 6 BUE attached to a chip machined at 5 m/min (tool is overlapped on image for clarification).

alt-text: Fig. 6

As seen from Fig. 5, at the speed of 50 m/min the lamellae start to lose their integrity, breaking apart into smaller grains. This process is most pronounced close to the rake surface where almost equiaxial grains are visible, while deeper into the chip the lamellar structure is preserved. At the higher cutting speeds the region of equiaxiality extends deeper into the chip to about 10 ~~micrometers~~ µm depth (dependence of the thickness of this region from the cutting speed is plotted at Fig. 8). It is notable that the size of the equiaxial grains increases from the surface to the depth of the chip from sub-100 nm to a few hundred nanometers across.

Fig. 7 presents the data obtained by the analysis of EBSD patterns. The upper row shows color coded orientation maps of SSZ of the chips cut at different speeds. These maps confirm the observations made by FIB channeling contrast – starting from 50 m/min cutting speed a layer of equiaxial small crystals starts to develop at the rake surface of the chip, and its thickness increases with growing cutting speed. At the same time the size of the grains, which develop equiaxiality increases with growing speed. The varying distribution of grain sizes with the depth below the rake surface is also visible. The black color in the proximity of the rake surface at 200 m/min cutting speed indicates that the grain sizes in this region are below the resolution limit of EBSD, which was of the range of 100 nm.

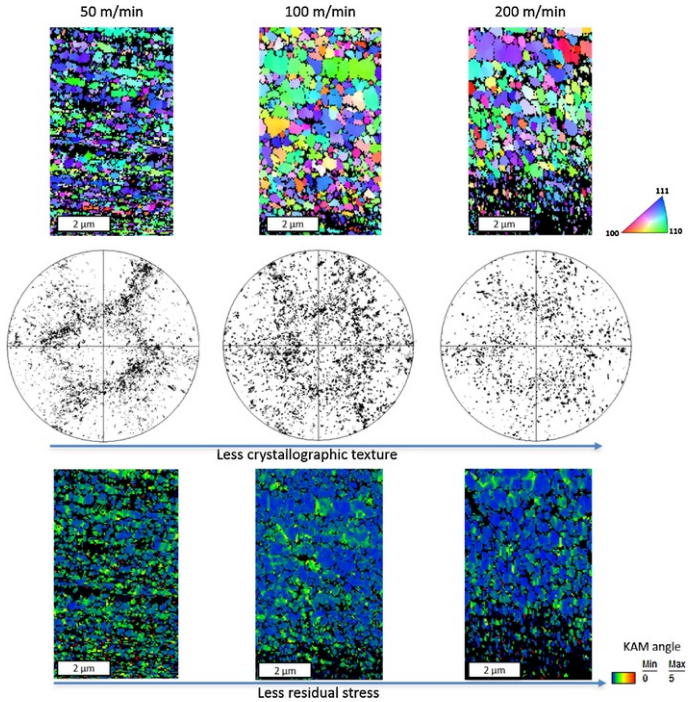

Fig. 7 Crystallographic orientation study by EBSD on SSZ (bottom of the images corresponds to chip-tool contact surface) on chips cut at 50, 100 and 200 m/min. Top row shows inverse pole figure (IPF) colored maps. The middle row plots the pole figures (PF). The bottom row represents the kernel average misorientation (KAM) maps.

alt-text: Fig. 7

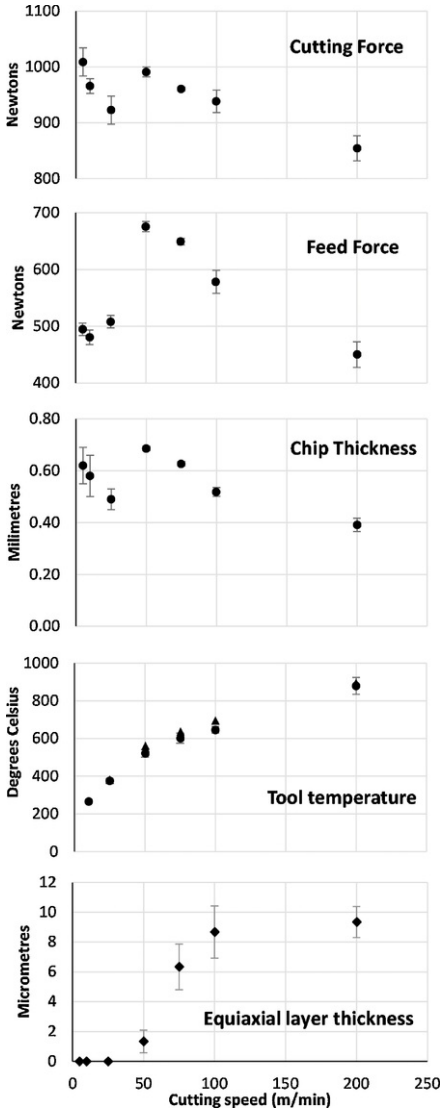

Fig. 8 Cutting force, feed force, chip thickness, tool temperature in chip-tool contact, and equiaxial grains layer thickness experimentally obtained by machining steel AISI 1045, feed 0.2 mm and cutting speed from 5 to 200 m/min. The error bars reflect the standard deviation of multiple measurements. Additionally the triangles on the tool temperature plot represent temperature values obtained in simulation (for cutting speed 200 m/min and above).

alt-text: Fig. 8

The polar maps in the middle row of Fig. 7 result from the statistical analysis of orientation maps and reflect the probability to find particular crystallographic orientation in the ensemble of crystals. Clustering of the points on these plots indicate the presence of preferential orientations/texture. As is seen on the middle row of Fig. 7 the pole figures become more diffused when the cutting speed grows from 50 to 200 m/min reflecting more stochastic distribution of the grains orientation. Thus an increase in cutting speed not only leads to disintegration of lamellae to small crystals, but also to rotation of these crystals inside the matrix. This can be also visually detected on the orientation maps at the top row of Fig. 7 as a more uniform color distribution with the increase of cutting speed.

The bottom row of Fig. 7 shows the outcome of kernel average misorientation (KAM) analysis of the same EBSD data. KAM represents the distortions of orientation inside individual grains, correlated by Calcagnotto et al. (2010)

to the density of geometrically necessary dislocations. The blue color on the KAM maps corresponds to relaxed grains, while green areas depict deformed regions. It is seen that lamellar structure is still present at 50 m/min, this cutting speed preserves many more dislocations than equiaxial grains obtained between 100 and 200 m/min. Thus, the process of lamellae disintegration leads also to a dissipation of stored defects and a relaxation of stored strain energy created upon shear deformation of SSZ.

As a summary of the microstructural study it can be concluded that the processes taking place at the tool-chip contact point develop different surface and microstructural morphologies in SSZ for chips generated below and above 50 m/min. This is related to the chip surface changing from cracked discontinuous to smooth, as well as the appearance of the subsurface area with an equiaxial crystallite morphology and reduced density of stored defects.

3.2 Machining output

In the experiments the forces, tool temperature, chip thickness and tool-chip contact length were measured for each cutting speed. The data obtained is depicted in Fig. 8 except for the tool-chip contact length, which is presented in the appendix. In-line with the machining output data, the thickness of the layer with equiaxial grains determined from FIB images is also plotted on Fig. 8 (see appendix for the method of measuring this thickness).

The cutting and feed forces, along with the chip thickness show a general decreasing trend with increasing cutting speed. However, this tendency presents a sharp transition. Between 25 and 50 m/min the cutting force abruptly increases by 10 %, recovering the decreasing trend further on. The feed force also has a transition between 25 and 50 m/min. Between 5 and 25 m/min the force remains constant, and at 50 m/min it increases by 33 ~~%. From 50 m/min onwards it monotonically reduces with the increase of cutting speed. The values of chip thickness present a similar feature between 25 and 50 m/min at which point the thickness increases by 50~~ %. From 50 m/min onwards it monotonically reduces with the increase of cutting speed. The values of chip thickness present a similar feature between 25 and 50 m/min at which point the thickness increases by 50%. This feature coincides with the onset of the formation of a layer of equiaxial grains. The temperature shows a monotonic growth without features reaching about 550℃ at 50 m/min.

4 Discussion

4.1 Compliance with the literature data

The trend in forces and chip thickness shown above is consistent with the transition described by Childs et al. (2000), from a cutting regime where the chip slides against the BUE, to the regime where the chip slides directly against the cutting tool. Confirmation for the existence of BUE at low cutting speeds is found in a detached BUE structure trapped in the chip at 5 m/min (Fig. 6). The abrupt transition observed between these two regimes at about 50 m/min· is in a good agreement with the results of Childs et al. (2000). However, Kümmel et al. (2014) observed a gradual reduction of BUE size at higher velocities in the range of 50 to 100 m/min, which may be related to a very small feed rate used in that study, resulting in lower temperatures at the tool. A simple picture for the feature in the behavior of macro-mechanical parameters observed experimentally has been provided by Childs (2013), where from simulations of the flow velocities in the chip it is evident that the BUE acts as a virtual tool tip, effectually increasing the rake angle. Thus the BUE, shown on Fig. 6, increases the effective rake angle from 6 to 20 degrees reducing the cutting force (F_c) by 8% and the feed force (F_f) by 35%, as well as chip thickness by 40%. Arrazola (2003) predicted an increase of approximately 1 (Please delete the space between 2 and %) ~~2 % and 5~~ 2 % and 5 10 % for cut and feed forces respectively for every 1 ~~degree~~ ° of decrease of the rake angle. For our case this would mean an expected increase of forces by 14 (Please delete the space between 28 and %) ~~28 % and 70~~ 28 % and 70 140 % for cut and feed forces respectively. There is an obvious two fold discrepancy between expectations and observations. In the same way, Childs (2013) has reported an approximately 2-fold discrepancy of experimental and simulated values for force increase during transition. Both estimations of Arrazola (2003) and Childs (2013) took into account the change in temperature softening due to change of the conditions in the cutting area, though this seems to be not sufficient to explain the experimentally observed small growth of forces. There should exist another and stronger softening mechanism, which switches on during transition and results in a substantial reduction of friction.

The structure of the BUE has been under extensive investigation by Kümmel et al. (2014) and Fig. 6 is consistent with their results. BUE has a very fine lamellae structure with the lamellae thickness down to 100 nm scale indicating high values of strain in this region. Due to the strain hardening of the material (which may reach 200 ~~–~~ 300 % according to Kümmel et al. (2014)) the BUE is harder than the workpiece and the rest of the chip, and thus can act as an effective tool tip as discussed above.

On the other side of the transition, i.e. above the 50 m/min cutting speed, a white layer under the rake surface of the chip, which is microscopically composed of equiaxial grains with a size down to the sub-100 nm scale and a random crystallographic orientation is observed. This is consistent with results of Sakai et al. (2014) on the structure of white layers obtained for different types of strain loads for different materials. Landau et al. (2016) associated the genesis of this sub-surface region with high strain, high strain rate and elevated temperature in localized points of the material. The origin of the layer was controversially discussed in terms of phase transition by Subramanian et al. (2002) or dynamical recrystallization (DRX) Sakai et al. (2014). By now it is well accepted that the equiaxiality and random orientation of sub-micrometer crystallites in this layer is achieved via rotational DRX, as described by Perez-Prado et al. (2001). Based on that, Meyers et al. (2003) suggested that DRX may take place at a notable rate already at the half melting temperature (in Kelvin) – this is close to the transition temperature observed in our experiments (see Fig. 8).

4.2 Origin of the BUE to non-BUE transition

A number of hypotheses have been proposed to describe the transition between two cutting regimes. Iwata and Ueda (1980) have proposed that the increase of temperature avoids cracks necessary to form the BUE. On the other hand, Childs (2013) suggested that over the blue-brittle temperature in steels the BUE cannot be sustained. These theories utilize the effect of thermal softening, i.e. gradual reduction of the strength of a material with the increasing temperature as described by Campbell and Ferguson (1970). This would lead to a scenario in which the secondary shear zone gradually becomes softer and thus less and less able to support the BUE. At the same time tribological experiments of Ben Abdelali et al. (2012) showed that in the similar cutting speed range a friction coefficient of AISI 1045 steel abruptly decreases more than twice. In a later work Ben Abdelali et al. (2013) found a clear correlation between tribological measurements and the appearance of the white layer. Though they still attributed the decrease of friction to thermal softening of the steel, these results clearly showed that the observed transition corresponds to a qualitative change of the friction mechanism. The friction at low speed is determined by plastic deformation in the contact layer, while at higher velocities plastic deformation is accompanied by DRX and thus dynamical microstructural softening. The later overwhelms the effect of thermal softening according to Landau et al. (2016), leading to a step-like increase of ductility. In this scenario, the temperature, rather than acting as a direct softening factor, triggers the DRX and thus dynamically creates a soft “lubricant” layer between the tool and the workpiece. Thus DRX is a missing piece of a puzzle which can explain the discrepancy between observed and predicted force increase after transition from the BUE to a direct sliding mode.

In this study the same mechanism is proposed to be responsible for the initiation of the transition between BUE and non-BUE regimes in orthogonal cutting experiments. In order to clarify a possible contribution of DRX in the change of cutting regimes the conditions for the DRX onset and evolution are discussed in more detail below.

4.3 DRX initialization and evolution in orthogonal cutting

DRX is a very common phenomenon under conditions where crystalline materials are subjected to high strains at high strain rates and elevated temperatures. It has been argued by Hines and Hines (1997), that DRX taking place in metals during high speed processing (punching, hot rolling, high speed cutting) has a rotational nature as opposed to migrational recrystallization. The time frames for the latter are a few orders of magnitude larger than for the former and there is simply not enough time for substantial boundary migration (governed by lattice diffusion) during a few milliseconds, which is a typical timescale in high speed processing; for instance in our experiments tool-chip contact time at 5 m/min is approximately 33 milliseconds, at 25 m/min - 7 milliseconds, at 50 m/min - 3.4 millisecond~~ms, at 25 m/min – 7 ms, at 50 m/min ×3.4 ms~~ms, at 25 m/min is 7 ms, at 50 m/min is 3.4 ms(Please delete: "milliseconds, at 25 m/min - 7 milliseconds, at 50 m/min - 3.4 millisecond", which is replaced for "ms, at 25 m/min is 7 ms, at 50 m/min is 3.4 ms"), and at 200 m/min is 0.46~~ millisecond~~ ms (see appendix for details of estimation of contact time). Rotational recrystallization in turn is governed by boundary diffusion, which according to Frost and Ashby (1982) is much faster than the lattice one and typically has an activation energy twice as low. To describe the onset of DRX in orthogonal cutting a simple model proposed by Meyers et al. (2003) for rotational DRX will be used. It is assumed here that DRX is a key and limiting stage in the process of material softening, i.e. all necessary preliminary steps, like dynamic recovery, take place before DRX onset without substantial time consumption. This is a reasonable assumption as the activation energy for these processes presented by Kuo and Lin (2007) is much lower than the one measured by Sakai et al. (2014) for DRX. Meyers et al. (2003) have described the rotation angle of a grain boundary during rotational DRX as

$$f(\theta) = \frac{4\delta D\gamma}{LkT}t \quad \textbf{(1)}$$

where $f(\theta)$ is a complex function of rotation angle θ only, δD is a product of grain boundary thickness and grain boundary diffusion coefficient, γ is the surface energy, L is the length of the grain face, k is a Boltzmann constant, T is the temperature and t is the duration of the process. δD is defined via grain boundary mobility δD_0 as:

$$\delta D = \delta D_0 exp\left(-\frac{Q}{RT}\right) \quad \textbf{(2)}$$

where Q is an activation energy for grain boundary diffusion and R is a gas constant.

Though parameter L in Eq. (1) is not exactly the grain size, it can be used if the relative comparison is made. Resolving Eq. (1) relative to L and combining it with Eq.~~(2) the following equation is obtained.(3)~~ (2) the following equation is obtained:

$$L = \frac{4\delta D_0 exp\left(-\frac{Q}{RT}\right)\gamma}{f(\theta)kT}t \quad \textbf{(3)}$$

which describes the size of the grains accessible to rotational DRX at particular temperature over the time period t.

The parameters used in the equations above for α-Fe are: values proposed by Frost and Ashby (1982) for the product of grain-boundary mobility and thickness $\delta D_0 = 1.1 \times 10^{-12}$ m^3/s and activation energy for grain-boundary diffusion $Q = 174$ kJ/mol, and a value proposed by Schönecker et al. (2015) for surface energy at 300 K $\gamma \sim 2.4$ J/m^2.

The function $f(\theta)$ has a singularity at 30° (at complete relaxation), so it is not convenient to deal with. For further discussion any other value close to 30° will rather be used, for example 29°, and DRX evolution for different

size of the crystallites will be monitored.

Fig. 9 shows the plot of ~~equation (3) for f(29°~~Eq. (3) for *f*(29°) calculated for the process time *t* interpolated from experimental data (between 0.5 and 33 ms, see appendix for details). The function has a smooth onset at about 400°C indicating that around this temperature DRX starts for the smaller sub-100 nm grains structurally leading to equiaxial nanocrystallites with random orientation. What is more important, according to Osovski et al. (2012) DRX results in dynamical softening of the material, which undergo recrystallization. Figs. 4 and 5 show that at low cutting speeds the finest anisotropic/lamellae crystals are found in SSZ at the proximity of the rake surface and also they constitute the BUE. So the onset of DRX will start in this region, making it softer than the rest of the material and thus efficiently preventing the formation of BUE.

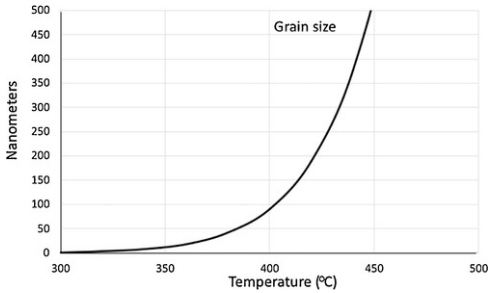

Fig. 9 The size of the grains accessible to rotational DRX (L in Eq. (3)) vs temperature.

alt-text: Fig. 9

With the increasing cutting speed the size of the crystallites accessible by DRX grows exponentially, which should seemingly lead to recrystallization of the whole chip. However, as is evident from the top row of Fig. 10 (numerical values obtained from the FEM simulations described in chapter 2), with growing cutting speed high temperatures become more and more localized close to the rake surface of the chip. The bottom row of Fig. 10 represents these temperature distributions recalculated in accordance to Eq. (3), i.e. it represents the distributions of the sizes of the crystallites accessible to rotational DRX at different cutting speeds. Simulation for 25 m/min was done assuming chip sliding against the tool without accounting for formation of BUE. As is seen from this simulation, if the chip was really sliding directly against the tool, the crystallites accessible to DRX would be less than 5 nm in size, meaning that practically DRX does not take place at this cutting speed; on the contrary, the strain hardening develops leading to the formation of BUE at these conditions. Starting from 50 m/min DRX acts on larger and larger grains, yet staying confined in 10–20 μm rake subsurface region even at highest velocities. This observation is in a close agreement to the observed saturation of the equiaxial layer thickness to the value of about 10–15 μm at high cutting speeds (Fig. 8).

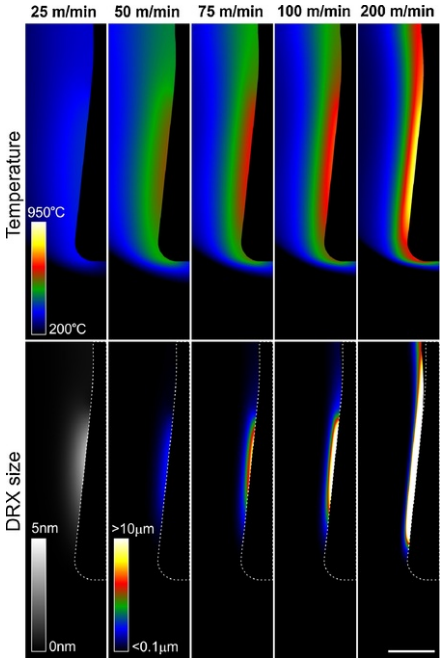

Fig. 10 Upper row – simulated temperature distribution in the chip for different cutting speeds assuming a direct sliding mode. Lower row – the map of crystal sizes accessible to rotational DRX calculated from temperature distributions according to Eq. (3). The scale bar corresponds to 100 μm for all images. Note a different color codding for the bottom left image.

alt-text: Fig. 10

It is remarkable that the grain size does not increase in the proximity of the contact as a result of DRX as is evident from Fig. 5 and especially from Fig. 7. This gives a strong argument for the rotational nature of DRX, which simply converts crystals severely elongated due to the shear stress into equiaxial grains of similar dimensions. Grain boundary migration, which would be responsible for the grains growth, is still not activated at these temperatures as was pointed out by Capdevila et al. (2003) for steel and Taheri et al. (2005) for aluminum.

4.4 Combined description of two cutting regimes

Thus, the role and evolution of DRX in orthogonal dry cutting of AISI 1045 steel may be qualitatively described as follows: The temperature threshold for the onset of rotational DRX separates the cutting conditions into two distinct regimes. Surprisingly, this threshold is very well described by the simple model of Meyers et al. (2003) for rotational DRX utilizing activation energy for grain boundary diffusion. If cutting conditions (besides the cutting speed this can be a feed rate, which was not studied in this work) are so, that the threshold temperature is not reached, the extreme shear stress in the SSZ leads to strain hardening of the rake surface of the chip, which sticks to the surface of the tool and promotes the growth of a BUE. The BUE then acts as an effective tool tip, increasing the rake angle and thus decreasing the forces acting on a tool. Instability of the BUE and its periodic detachment can result in a rough surface of the chip (and the workpiece, which was not shown in this work).

When the temperature threshold is reached, the dynamic softening due to DRX first develops at the very proximity of the contact between the chip and the tool, thus canceling the strain hardening and preventing the formation of a BUE. As is seen from Fig. 10, conditions for DRX are first reached not directly on the tip itself, but at some distance up the tool rake surface, which may lead to a gradual decrease of the BUE size with cutting speed (as was observed e.g. by Kümmel et al. (2014)), rather than to an abrupt transition. It should be pointed out, that even at the highest cutting speed studied in this work (200 m/min), the area close to the tool tip is not accessible by DRX and thus the tool surface is always in contact with the strain hardened material, though the area of this contact decreases at higher speed.

The transition from BUE mode to the direct sliding of the chip against the tool surface is accompanied by a decrease of the effective rake angle (in our case from 20 to 6 degrees as was discussed in ~~s~~Section 4.1) leading to the stepwise increase of cutting forces and an increase of chip thickness. With a further increase of the cutting speed the thickness of the soft DRX layer (which acts as a lubricant) increases together with the temperatures at the SSZ, leading to a gradual decrease of the cutting forces and chip thickness. The thickness of DRX layer saturates already at 200 m/min due to a strong localization of high temperature near chip-tool interface. The micro-nano-structure of

the DRX layer, namely preservation of the size of the crystallites during recrystallization, gives a strong argument for the purely rotational nature of DRX process.

5 Conclusions

The area of the secondary shear zone that develops dynamic recrystallizations has been matter of a multi-approach analysis. Morphological, structural and mechanical studies have been elucidated.

Samples of AISI 1045 steel were studied under machining at cutting speeds between 5 and 200 m/min. The combination of several information sources, from the machining tests to the ion scanning microscopy, successfully revealed the succession of events that drives the chip flow regime at mid-high cutting speeds.

- The change of the cutting mode at a speed between 25 and 50 m/min was observed for the orthogonal dry cutting of AISI 1045 steel with uncoated P15 carbide cutting tools, which reflected in the abrupt change of cutting forces, chip thickness and chip microstructure. According to the concepts existing in the literature this change was attributed to a transition between the BUE formation mode and the direct sliding mode.
- The microstructure observed in the chips produced below the transition speed was characteristic for cold working, and showed drastically strained lamellae structure in the SSZ. Chips produced over the transition speed showed the presence of the layer of equiaxial grains down to 100 nm size, which is characteristic for the DRX process. The independence of the grain size in relation to the cutting speed pointed to the rotational nature of the DRX.
- It was proposed that it is a temperature onset of the DRX which causes the transition from the BUE to the non-BUE mode and described a complete scenario of the transition between the two modes.
- FE simulations reproduced the onset and further evolution of the DRX layer, demonstrating that the onset of DRX coincides with the activation of the grain boundary diffusion, which is an underlying mechanism for rotational recrystallization.

The potential of the complex approach including systematic microstructural characterization for understanding of the processes taking place in the confined space and at the extreme conditions during orthogonal cutting was demonstrated. The present study provides new insights into the machining process, alluding to fundamental microstructural effects to explain the evolution of the tool-chip contact. This could help solving tool-chip friction issues in future simulations and practical experiments.

Declarations of interest

None.

Acknowledgements

The authors thank the projects MICROMAQUINTE (PI_2014_1_116) and EMULATE (DP12015-67667-C3-3R) for their funding of the research presented in this paper. The authors also wish to acknowledge project PI2014_1_79 for supporting this research. They also express their sincere thanks to Jorge Rafael Velayarce (MWW, Saarland University) and Christopher Tollan (CIC NanoGUNE).

Appendix A. Supplementary data

Supplementary material related to this article can be found, in the online version, at doi:https://doi.org/10.1016/j.jmatprotec.2018.05.016.

References

Armendia M., Garay A., Villar A., Davies M.A. and Arrazola P.J., High bandwidth temperature measurement in interrupted cutting of difficult to machine materials, *CIRP Ann. - Manuf. Technol.* **59**, 2010, 97–100, https://doi.org/10.1016/j.cirp.2010.03.059.

Arrazola P.-J., Aristimuno P., Soler D. and Childs T., Metal cutting experiments and modelling for improved determination of chip/tool contact temperature by infrared thermography, *CIRP Ann. - Manuf. Technol.* **64**, 2015, 57–60, https://doi.org/10.1016/j.cirp.2015.04.061.

Arrazola P.J., Modélisation Numérique de la Coupe: Étude de Sensibilité des Paramètres d'Entrée et Identification du Frottement entre Outil-Copeau, 2003, Universite de Nantes.

Arrazola P.J., Villar a, Ugarte D. and Marya S., Serrated ~~Chip Prediction in Finite Element Modeling of the Chip Formation P~~chip prediction in finite element modeling of the chip formation process, *Mach. Sci. Technol.* **11**, 2007, 367–390, https://doi.org/10.1080/10910340701539882.

Ben Abdelali H., Ben Salem W., Rech J., Dogui A. and Kapsa P., Characterization of the ~~Friction Coefficient and White Layer at the Tool-Chip-Workpiece Interface Using Experimental and Numerical Studies during Friction T~~friction coefficient and white layer at the tool-chip-workpiece interface using experimental and numerical studies during friction tests of AISI 1045, *Lect. Notes Mech. Eng.* **1**, 2013, 69–77, https://doi.org/10.1007/978-3-642-37143-1

Ben Abdelali H., Claudin C., Rech J., Ben Salem W., Kapsa P. and Dogui A., Experimental characterization of friction coefficient at the tool-chip-workpiece interface during dry cutting of AISI 1045, *Wear* **286–287,**, 2012, 108–115, https://doi.org/10.1016/j.wear.2011.05.030.

Calcagnotto M., Ponge D., Demir E. and Raabe D., Orientation gradients and geometrically necessary dislocations in ultrafine grained dual-phase steels studied by 2D and 3D EBSD, *Mater. Sci. Eng. A* **527**, 2010, 2738–2746 https://doi.org/10.1016/j.msea.2010.01.004.

Campbell J.D. and Ferguson W.G., The temperature and strain rate dependence of the shear strength of mild steel, *Philos. Mag.* **21**, 1970, 63–82.

Canovic S., Jonsson T. and Halvarsson M., Grain contrast imaging in FIB and SEM, *J. Phys. Conf. Ser.* **126**, 2008, 12054, https://doi.org/10.1088/1742-6596/126/1/012054.

Capdevila C., Chen Y.L., Jones a.R. and Bhadeshia H.K.D.H., Grain ~~Boundary Mobility in Fe-Base Oxide Dispersion Strengthened PM2000 A~~boundary mobility in Fe-base oxide dispersion strengthened PM2000 alloy, *ISIJ Int.* **43**, 2003, 777–783, https://doi.org/10.2355/isijinternational.43.777.

Childs T.H.C., Ductile shear failure damage modelling and predicting built-up edge in steel machining, *J. Mater. Process. Technol.* **213**, 2013, 1954–1969, https://doi.org/10.1016/j.jmatprotec.2013.05.017.

Childs T.H.C., Maekawa K., Obikawa T. and Yamane Y., Metal Machining, Theory and ~~a~~Applications, 2000, Elsevier.

Courbon C., Mabrouki T., Rech J., Mazuyer D., Perrard F. and D'Eramo E., Towards a ~~Physical FE Modelling of a Dry Cutting Operation: Influence of Dynamic Recrystallization When M~~physical FE modelling of a dry cutting operation: influence of dynamic recrystallization when machining AISI 1045, *Procedia CIRP* **8**, 2013, 516–521, https://doi.org/10.1016/j.procir.2013.06.143.

Frost H.J. and Ashby M.F., Deformation-~~mechanism maps : the plasticity and creep of metals and c~~Mechanism Maps: the Plasticity and Creep of Metals and Ceramics, 1982, Pergamon Press; Oxford [Oxfordshire]; New York.

Griffiths B.J., Mechanisms of White ~~Layer Generation With Reference to Machining and Deformation P~~layer generation with reference to machining and deformation processes, *J. Tribol.* **109**, 1987, 525, https://doi.org/10.1115/1.3261495.

Hines J.a. and Hines J.a., Recrystallization kinetics within shear bands adiabatic, *Acta Metall.* **45**, 1997, 635–649.

Iwata K. and Ueda K., Fundamental analysis of the mechanism of built-up edge formation based on direct scanning electron microscope observation, *Wear* **60**, 1980, 329–331.

Jaspers S.P.F.C. and Dautzenberg J.H., Material behaviour in metal cutting: ~~S~~strains, strain rates and temperatures in chip formation, *J. Mater. Process. Technol.* **121**, 2002, 123–135, https://doi.org/10.1016/S0924-0136(01)01227-4.

Kümmel J., Gibmeier J., Müller E., Schneider R., Schulze V. and Wanner A., Detailed analysis of microstructure of intentionally formed built-up edges for improving wear behaviour in dry metal cutting process of steel, *Wear* **311**, 2014, 21–30, https://doi.org/10.1016/j.wear.2013.12.012.

Kuo C.-M. and Lin C.-S., Static recovery activation energy of pure copper at room temperature, *Scr. Mater.* **57**, 2007, 667–670, https://doi.org/10.1016/j.scriptamat.2007.06.054.

Landau P., Osovski S., Venkert A., Gartnerova V. and Rittel D., The genesis of adiabatic shear bands, *Sci. Rep.* **6**, 2016, 3726, https://doi.org/10.1038/srep37226.

Lee S., Hwang J., Shankar M.R., Chandrasekar S. and Compton W., Large strain deformation field in machining, *Metall. Mater. Trans. A* **37**, 2006, 1633–1643, https://doi.org/10.1007/s11661-006-0105-z.

Meyers M.A., Xu Y.B., Xue Q., Pérez-Prado M.T. and McNelley T.R., Microstructural evolution in adiabatic shear localization in stainless steel, *Acta Mater.* **51**, 2003, 1307–1325, https://doi.org/10.1016/S1359-6454(02)00526-8.

Osovski S., Nahmany Y., Rittel D., Landau P. and Venkert A., On the dynamic character of localized failure, *Scr. Mater.* **67**, 2012, 693–695, https://doi.org/10.1016/j.scriptamat.2012.07.001.

Perez-Prado M.T., Hines J.A. and Vecchio K.S., Microstructural evolution in adiabatic shear bands in Ta and Ta-W alloys, *Acta Mater.*, 2001, https://doi.org/10.1016/S1359-6454(01)00215-4.

Pu C.L., Zhu G., Yang S., Yue E.B. and Subramanian S.V., Effect of microstructure softening events on the chip morphology of AISI 1045 steel during high speed machining, ~~*The International Journal of Advanced Manufacturing Technology*~~ *Int. J. Adv. Manuf. Technol.* 2015, 2149–2155, https://doi.org/10.1007/s00170-015-7472-9.

Rech J., Arrazola P.J., Claudin C., Courbon C., Pusavec F. and Kopac J., Characterisation of friction and heat partition coefficients at the tool-work material interface in cutting, *CIRP Ann. - Manuf. Technol.* **62**, 2013, 79–82, https://doi.org/10.1016/j.cirp.2013.03.099.

Saez-de-Buruaga M., Esnaola J.A., Aristimuno P., Soler D., Björk T. and Arrazola P.J., ~~. A Coupled Eulerian Lagrangian Model to Predict Fundamental Process Variables and Wear Rate on Ferrite-pearlite S~~A coupled eulerian lagrangian model to predict fundamental process variables and wear rate on ferrite-pearlite steels, *Procedia CIRP* **58**, 2017, 251–256, https://doi.org/10.1016/j.procir.2017.03.194.

Sakai T., Belyakov A., Kaibyshev R., Miura H. and Jonas J.J., Dynamic and post-dynamic recrystallization under hot, cold and severe plastic deformation conditions, *Prog. Mater. Sci.* **60**, 2014, 130–207, https://doi.org/10.1016/j.pmatsci.2013.09.002.

Schönecker S., Li X., Johansson B., Kwon S.K. and Vitos L., Thermal surface free energy and stress of iron, *Sci. Rep.* **5**, 2015, 14860, https://doi.org/10.1038/srep14860.

Seker U., Kurt A. and Çiftçi I., The effect of feed rate on the cutting forces when machining with linear motion, *J. Mater. Process. Technol.* **146**, 2004, 403–407, https://doi.org/10.1016/j.jmatprotec.2003.12.001.

Soler D., Aristimuño P., Garay A. and Arrazola P.J., Uncertainty of temperature measurements in dry orthogonal cutting of titanium alloys, *Infrared Phys. Technol.* **71**, 2015, 208–216, https://doi.org/10.1016/j.infrared.2015.04.001.

Soler D., Aristimuño P., Saez-de-Buruaga M., Garay A. and Arrazola P.J., New calibration method to measure rake face temperature of the tool during dry orthogonal cutting using thermography, *Appl. Therm. Eng.* **137**, 2018, 74–82, https://doi.org/10.1016/j.applthermaleng.2018.03.056.

Subramanian S.V., Gekonde H.O., Zhu G. and Zhang X., Role of ~~Microstructural Softening Events in Metal C~~microstructural softening events in metal cutting, *Mach. Sci. Technol.* **6**, 2002, 353–364, https://doi.org/10.1081/MST-120016250.

Taheri M.L., Molodov D., Gottstein G., Rollett a.D., Huang Y. and Humphreys F.J., Grain boundary mobility under a stored-energy driving force: a comparison to curvature-driven boundary migration, *Zeitschrift für Met* **96**, 2005, 1166–1170, https://doi.org/10.3139/146.101157.

Wallbank J., Structure of built-up edge formed in metal cutting, *Met. Technol.* **6**, 1979, 145–153, https://doi.org/10.1179/030716979803276426.

Appendix A. Supplementary data

The following are Supplementary data to this article:

Multimedia Component 1

Graphical abstract

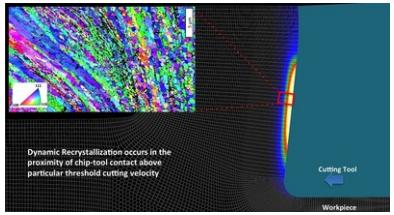

Queries and Answers

Query: Fig. 4 will appear in black and white in print and in color on the web. Based on this, the respective figure caption has been updated. Please check, and correct if necessary.

Answer: Authors agree with the update.

Query: Your article is registered as a regular item and is being processed for inclusion in a regular issue of the journal. If this is NOT correct and your article belongs to a Special Issue/Collection please contact c.norris@elsevier.com immediately prior to returning your corrections.
Answer: This is article is a regular item.

Query: The author names have been tagged as given names and surnames (surnames are highlighted in teal color). Please confirm if they have been identified correctly.
Answer: Yes

Query: Please check the journal title added in Ref. “Pu et al., 2015” and correct if necessary.
Answer: The cited article is the correct one.